IMPROVED REGIONAL SEISMIC EVENT LOCATIONS USING 3-D VELOCITY MODELS

Delaine Reiter
Shirley Rieven
Michelle Bernard
Weston Geophysical Corporation
325 W. Main Street
Northboro, MA 01532

William Rodi
Carolynn Vincent
Earth Resources Laboratory
Massachusetts Institute of Technology
42 Carleton Street
Cambridge, MA 02142

Phase I Final Report
Small Business Innovative Research Program
Defense Threat Reduction Agency, Topic DTRA99-012

REPORT DOCUMENTATION PAGE

Form Approved OMB No. 0704-0188

1. AGENCY USE ONLY (*Leave blank*)	2. REPORT DATE	3. REPORT TYPE AND DATES COVERED
DTRA01-99-M-0429	December 15, 1999	Final Report

4. TITLE AND SUBTITLE
Improved Regional Seismic Event Locations Using 3-D Velocity Models

5. FUNDING NUMBERS

6. AUTHORS Delaine Reiter, William Rodi, Shirley Rieven, Michelle Bernard, Carolynn Vincent

7. PERFORMING ORGANIZATION NAME(S) AND ADDRESS(ES)
Geophex, Ltd. dba Weston Geophysical
325 W. Main Street
Northboro, MA 01532

8. PERFORMING ORGANIZATION REPORT NUMBER

9. SPONSORING/MONITORING AGENCY NAME(S) AND ADDRESS(ES)

10. SPONSORING/MONITORING AGENCY REPORT NUMBER

11. SUPPLEMENTARY NOTES
Sponsored by the Defense Threat Reduction Agency, under Contract No. DTRA01-99-M-0429

12a. DISTRIBUTION/AVAILABILITY STATEMENT
Approved for public release; distribution is unlimited.

12b. DISTRIBUTION CODE

13. ABSTRACT(*maximum 200 words*)

Report developed under SBIR contract for topic DTRA99-012.

The objective of this research is to develop improved methods for regional and local seismic event locations from 3-D velocity models. Improved hypocenter estimates and high-resolution velocity models are critical to the successful seismic monitoring of potential nuclear tests. During Phase I of the study we have developed a nonlinear, multiple event location technique which uses primary and secondary phases (for P waves) and a 3-D regional velocity model to estimate event hypocenters. Travel times for the regional phases are calculated using a sophisticated eikonal finite-difference scheme, and the locations are determined using an efficient grid-search algorithm for 3-D media. We demonstrate its capabilities using synthetic data and a 3-D velocity model from a region of US monitoring concern.

14. SUBJECT TERMS
Seismic Event Location, 3-D Grid Location Methods, SBIR Report

15. NUMBER OF PAGES

16. PRICE CODE

17. SECURITY CLASSIFICATION OF REPORT	18. SECURITY CLASSIFICATION OF THIS PAGE	19. SECURITY CLASSIFICATION OF ABSTRACT	20. LIMITATION OF ABSTRACT
Unclassified	Unclassified	Unclassified	

NSN 7540-01-280-5500

Standard Form 298 (Rev. 2-89)
Prescribed by ANSI Std. 239-18 298-102

Contents

List of Figures

1.0 INTRODUCTION

The primary objective of this Phase I project was to demonstrate the use of a powerful technique to determine hypocenter estimates from the arrival times of regional or local seismic body waves and 3-D velocity models. We have focused on the development of a grid-search based, nonlinear hypocenter inversion technique which can greatly improve estimates of event locations. Our algorithm calculates travel times using a finite difference approximation of the eikonal equation (Podvin and Lecomte, 1991). The location algorithm determines the event hypocenters by performing a search over a 3-D grid of potential hypocenters to minimize arrival time residuals. We have modified the travel time prediction algorithm to begin exploiting secondary regional phase travel times and have begun optimizing the grid-search location algorithm for the regional monitoring problem. In this paper we will report on the method's capabilities in a regional seismic monitoring application using synthetic data and a preliminary 3-D velocity model we have built for the Pakistan/India region under other work funded by the Defense Threat Reduction Agency.

1.1 Background

Current national monitoring goals require the accurate location and characterization of seismic events with a high degree of confidence. The global extent of the monitoring efforts, which requires the swift detection and identification of large numbers of small magnitude events, requires the development of new capabilities to analyze regional seismic data. A critical step in correctly identifying a seismic event is the determination of an accurate source location. Certain regions of the world have been adequately instrumented and calibrated to produce location estimates with high accuracy. But in many other regions, systematic errors due to a lack of regional location calibration information can cause significant deviations between the calculated and true source locations. There are two predominant ways to improve the location of a seismic event. One is to use reliable path calibrations developed from events of known location. The other method is to use high-resolution, 3-D models of the Earth's velocity structure for predicting travel times in the location process. The latter method is ultimately preferable because of the obvious side benefits that accompany it, such as the ability to use the 3-D model in characterizing the uncertainty of the final location estimate. Models of the Earth can never account for all the complexity seen in seismic data, but sufficiently detailed models of specific regions of interest can be constructed to produce locations accurate enough for regional seismic monitoring.

1.2 Nonlinear Event Location Using 3-D Velocity Models

Finding the precise location of an earthquake or a man-made seismic event has been a problem of long-standing interest to seismologists. All methods of seismic event location require

the prediction of travel times between an event hypocenter and the recording stations, using some form of a velocity model between the event and the station. Hypocentral locations are then estimated through the minimization of the travel time residuals between the observed and calculated arrival times. The current location procedure at the Prototype International Data Center (PIDC) uses a conventional least-squares algorithm to locate seismic events. In addition to the first-arriving and S phases, the PIDC incorporates a range of secondary phases (P_g, pP, sP, PcP, PP, etc.) as well as azimuth and slowness measurements obtained from both arrays and three-component stations. However, the PIDC is currently limited to using global travel time tables (IASP91) in most regions of the world (GSE Conference Room Paper 243, 1995), although methods to incorporate station corrections, regional travel time models, and path-dependent measurements are being tested. Other methods of seismic event location estimation have been developed in recent years which take advantage of computational advances such as grid-based ray tracing methods (Vidale, 1988; Moser, 1991; Podvin and Lecomte, 1991). These ray tracing methods, combined with sophisticated inversion techniques, have led to grid-search earthquake location algorithms capable of predicting hypocenters in 3-D media (Moser et al. 1992; Wittlinger et al., 1993; Lomax et al., 1998). The benefits of these methods are that they do not require the calculation of travel time derivatives near an estimated hypocenter (as do the traditional methods) and that they are less susceptible to instabilities in the numerical solution. Some of them are also able to handle complicated 3-D, regional velocity models, which are much more appropriate for the modern seismic monitoring problem in many cases. However, grid-based location algorithms still require improvements before they can become routinely useful in the regional monitoring problem. During Phase I of this research, we have developed a version of a grid-based location algorithm tailored to the regional monitoring setting. We have improved the accuracy of the travel time prediction algorithm using a multi-grid approach, incorporated some secondary phases in the location estimate, and increased the efficiency of the 3-D grid location technique. We have applied the new method to a synthetic data sets obtained by ray tracing through a preliminary 3-D model of the Pakistan region constructed for use in other work funded by the Defense Threat Reduction Agency. Each of these improvements will be discussed in the following sections.

2.0 RESEARCH ACCOMPLISHED

2.1 Task 1: Finite Difference Computation of Regional Travel Times

An essential component of any location algorithm is the ability to predict the travel times of seismic phases through a given velocity model. In the regional monitoring problem, lateral and 3-D heterogeneity in the crust precludes the use of traditional, global 1-D velocity models such as IASP91 or J-B. 3-D velocity models require more sophisticated travel time modeling routines; thus, we use a 3-D eikonal equation solver originally developed by Podvin and

Lecomte (1991). They extended the original method of Vidale (1988) in various ways. The Podvin-Lecomte algorithm (hereafter referred to as P-L) correctly takes into account the possibility that several locally independent wavefronts may contribute to the wavefield at any point in the medium. Multiple arrivals at any point are systematically considered, and a first arrival criterion is used to pick the one with the minimum travel time. The traditional eikonal equation methods do not account for multi-pathing, using instead a single-wavefront approximation in the propagation. This is the main reason why the traditional, Vidale-style finite difference algorithm cannot correctly handle large velocity contrasts. The P-L method can handle velocity contrasts as high as 1:10, no matter what the shape of the feature.

In the P-L algorithm, the velocity model is set up as a uniform Cartesian grid in three dimensions. The first arrival travel time is computed at each node of the grid from a source located within the grid. In our application, the "source" is actually taken to be a station and, owing to reciprocity, each node of the 3-D grid is the hypocenter of some event. The resulting grids, one for each station and phase, embody a set of 3-D travel time tables which can be used by an event location algorithm. The ability to compute travel times from one point (i.e. the station) to every other grid point is a great advantage that the eikonal solvers (and other grid methods) have over traditional bending and shooting methods. Travel times for S phases are calculated using a shear wave velocity grid, or S arrival times can be predicted from a pre-set Vp/Vs ratio. This method of travel time computation is considerably faster than two-point ray tracing when a large number of sources or receivers is involved, distributed throughout the model.

During Phase I, we adapted the P-L algorithm to the regional seismic monitoring setting. Several changes in the technique had to be implemented before the algorithm was suitable for our use. A major concern to address was the accuracy of the method when used in a regional monitoring scenario, where source-receiver distances are large. For example, a 1% error in the travel time of P_g at an epicentral 1000 km amounts to 2 seconds of error, sufficient to cause an unacceptable bias in the location of an event. To deal with this concern, we made changes in the initialization procedure to greatly increase the accuracy of the travel time estimates in the immediate region surrounding the source (i.e. the station, in our case). Local computations in the P-L method are based on a plane wavefront approximation, which near the source can be quite imprecise. To improve the accuracy of the method in the case where the source is in a heterogeneous zone, we have implemented a multi-grid approach. This entails extracting a cubic region surrounding the source and calculating travel times on a grid with much finer mesh spacing. The travel times from the nodes of the finer mesh common to the coarser grid are reinserted, and the algorithm proceeds to propagate the travel time grid to all nodes using finite differences. A schematic of this process is shown in Figure 1.

It was also necessary to adapt the P-L method to the regional setting by performing transformations of the velocity model and output times between geographic and Cartesian coordinates. The P-L code was originally written for local earthquake location studies, where

Figure 1: Schematic of the multi-grid process to increase the accuracy of the Podvin-Lecomte travel time prediction method.

curvature of the Earth could be safely ignored. Rather than completely rewriting the P-L code during Phase I, we have implemented flattening transformations on the velocity model prior to running the code and then "unflatten" the resulting travel time grids during the location procedure. The flattening equations are

$$z' = a\log(1 - z/a) \tag{1}$$
$$= a\log(a/r)$$
$$v' = v/(1 - z/a) \tag{2}$$
$$= v(a/r),$$

where z' and v' are the transformed depths and velocities that the P-L code uses. In addition, v, r and $z = a - r$ are the velocities and depths in the spherical earth, with $a = 6371km$. This procedure is exact for 1-D earth models and approximate for 3-D models.

After making these changes to the P-L algorithm, we performed extensive testing of the method to determine the accuracy for various velocity models. We did this prior to using the newly improved method on our strongly heterogeneous, preliminary 3-D model of the Pakistan region. The models we tested were a homogeneous half-space, a 2-layer model mimicking the velocity contrast between the crust and mantle, and the IASPEI91 1-D global velocity model to a depth of 410 km. Our goal was to produce travel time errors less than 0.5 seconds for all azimuths, source depths and epicentral distances to 2000 km. The tests were performed to determine algorithmic parameters such as optimal grid spacing in the coarse grid, the overall dimensions of the source-region initialization grid, and grid spacing in the source-region grid. Based on these tests, we are currently using 5 km ($h = 5$) spacing in the coarse regional grid, a overall source region size of $22h$ per side with the source point at the center node, and a source region grid spacing of 1 km. In all of the tests discussed below, we have designed the models to support the work we are doing on our regional Pakistan model. Therefore, we placed the source (station) at the location of NIL, the IMS station at the Earth's surface in Nilore, Pakistan, and propagated travel times on a grid encompassing our Pakistan regional model (461 nodes in longitude $\times$ 401 nodes in latitude $\times$ 17 nodes in depth. Essentially, the plots described below depict the travel time errors from sources at a given depth everywhere in the particular model to a station positioned at NIL (33.65°N, 73.2512°E). A summary of the results follows:

1. **Homogeneous model** — This model was produced as an initial test of the method because we can compare the results to the simple analytical solution. We display all the results in this report as differences in travel time between the P-L method and the analytical answer for horizontal slices through the resultant travel time grid. Figures 2 and 3 are slices from the travel time grid at 0 km depth and 60 km depth. The errors are all 0.4 seconds and under, with the largest errors concentrated along certain azimuths. Apparently, the travel times along raypaths passing through the corners or model cells are most accurate, while those that intersect cell faces are least accurate.

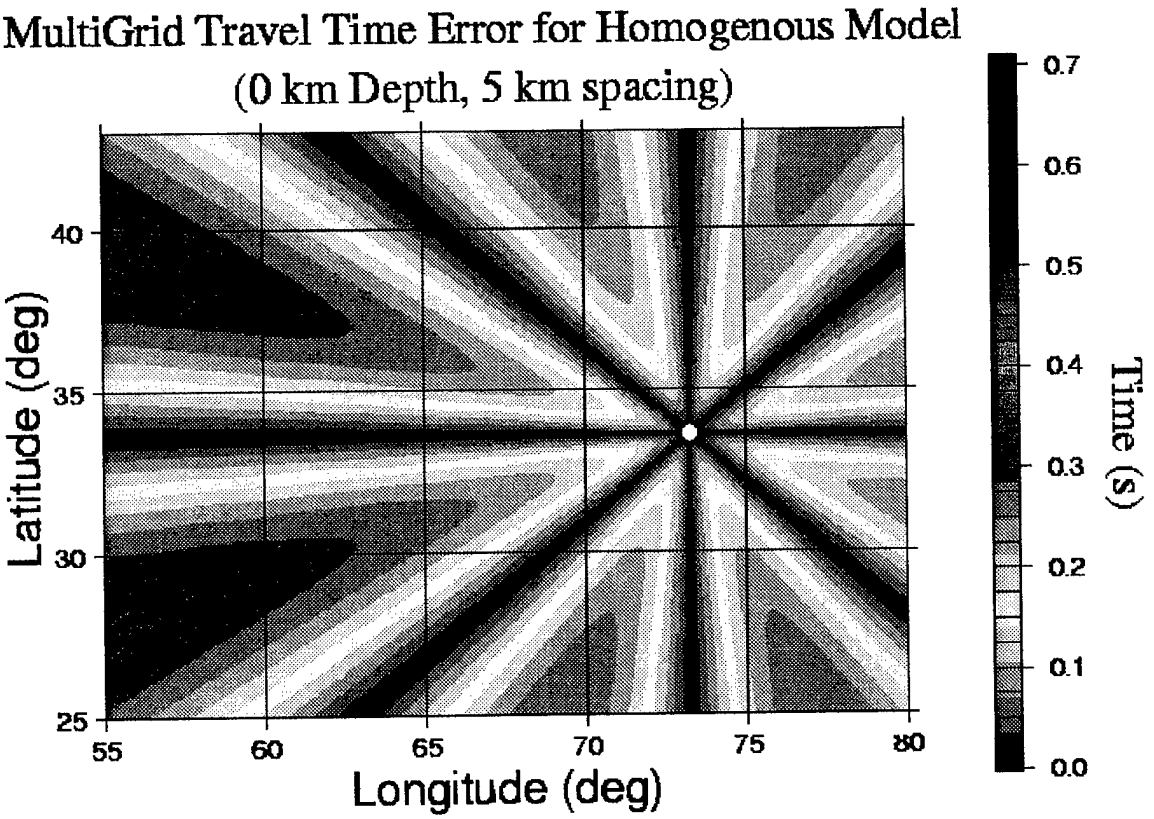

Figure 2: The travel time error for a homogeneous model (the difference between the P-L method and the analytical solution) for a source at 0 km depth on the depth surface $z = 0$ km of the grid). The maximum error is around .4 seconds.

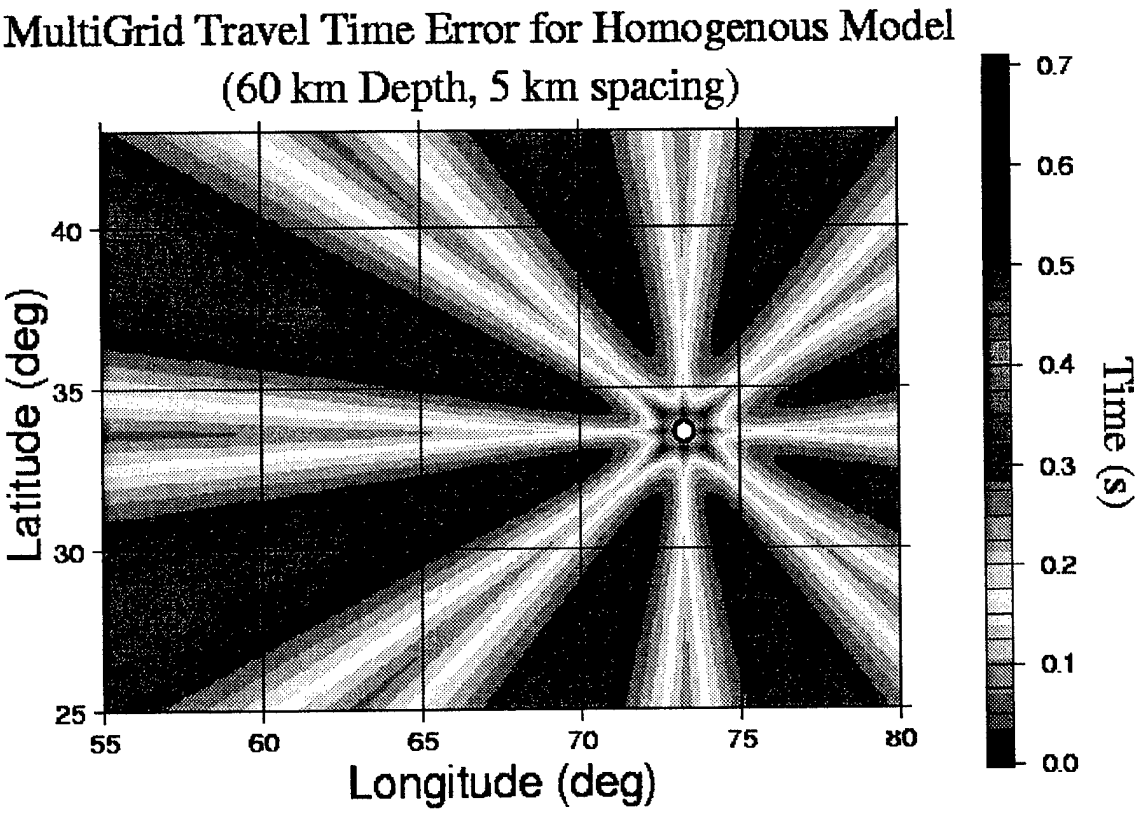

Figure 3: The travel time error for a homogeneous model (the difference between the P-L method and the analytical solution) for a source at 0 km depth on the depth surface $z = 60$ km of the grid). The maximum error is slightly over .4 seconds.

2. **Two layer (crust/mantle) model with flat interface** — This model consists of a 35 km thick layer of 6.0 km/s over a halfspace layer of 8.0 km/s. An analytical solution also exists for this example, and we have plotted the travel time surfaces from the grid at 0 km and 60 km depth (Figures 4 and 5). The narrow black ring surrounding the station in Figure 4 is an artifact of the chosen color scale, and consists of negative numbers very close to zero. It is related to the crossover distance between P_g and P_n. The absolute errors do not exceed approximately 0.3 seconds at any point in the grid.

3. **IASP91 1-D global model** — The IASPEI91 model is one of the currently used default models for location processing in IDC software and databases. Therefore, we tested the multi-grid version of the P-L code on the 1-D layered model using a similar set-up as with the previous test models. One exception to previous models was that we extended our Pakistan regional model to 410 km depth by blending it into the IASP91 model below 80 km, which is the maximum depth of the 3-D regional Pakistan model. Figures 6 and 7 depict the error surfaces in the travel time grid at 20 km and 60 km depth for a source sited at the location of the station NIL, as in the above examples. The errors are with respect to "analytic" IASP91 travel times generated by limearly interpolating the IASP91 P wave table (obtained from the Center for Monitoring Research) onto the same 3-D grid used in the P-L calculation. The 2-D IASP91 table is sampled only every one degree in distance and variably in depth (from 5 to 50 km depth spacing), so the times are not exact. This results in approximately a -1.3 second discrepancy in our P-L results at 20 km depth in a circle around the source at a distance corresponding to the P_g/P_n cross-over distance, which is not properly represented in the 1-degree sampled analytic P table. At 60 km, the branch of the travel time vs. distance curve corresponding to upgoing rays has significant concave-upward curvature, and this also is not well represented in the tables. Hence, there is approximately a -1.6 second discrepancy in a ring under the source. Ignoring these discrepancies, which are clipped in the plots, the we see that the errors in our P-L calculations are generally less than 0.5 seconds.

Following the accuracy tests on the simpler models, the P-L algorithm was also modified to produce travel time tables for secondary phases in our regional Pakistan model. For now we have concentrated on developing travel time tables for P_g, P_n and true mantle P phases, as these are by far the most frequently observed body wave phases in seismic event bulletins. The extension to S waves is fairly trivial, and we plan to implement this capability as the research continues. In the following paragraphs we describe our procedure for making travel time tables for P_g, P_n and P.

We adopt the convention that the "P wave" travel time table used for event location should contain, at each grid point, the travel time of the first arriving phase to that point.

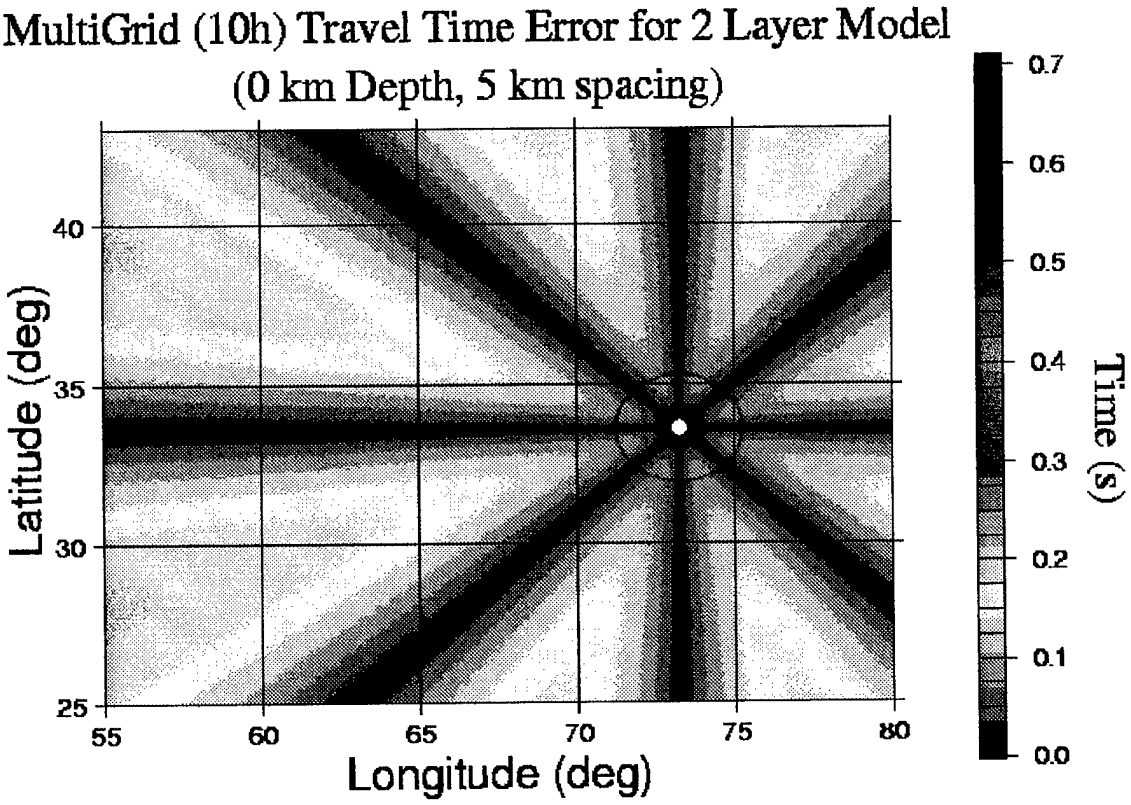

Figure 4: The travel time error between the P-L method and an analytical solution for a 2-layer model (35 km thick layer of 6.0 km/s over a halfspace of 8.0 km/s). The source is placed at the location of the station NIL, and the depth surface shown is $z = 0$ km slice of the grid. The absolute maximum error does not exceed .35 seconds.

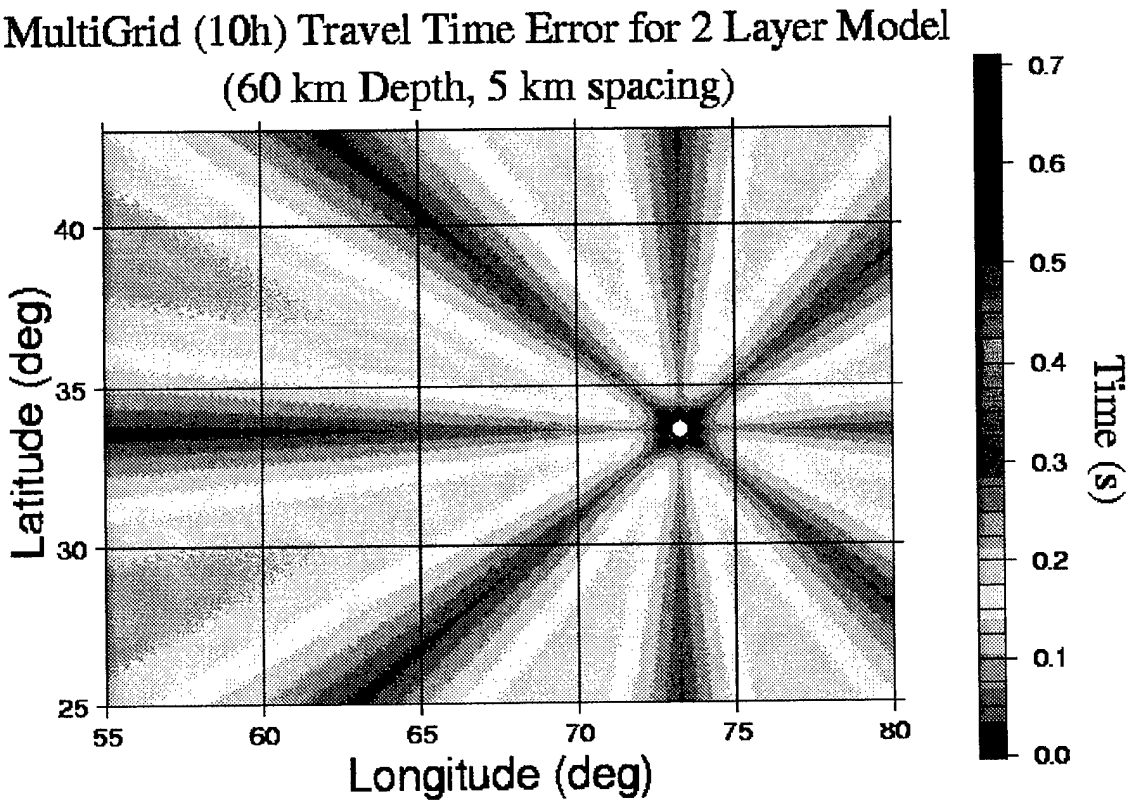

Figure 5: The travel time error between the P-L method and an analytical solution for a 2-layer model (35 km thick layer of 6.0 km/s over a halfspace of 8.0 km/s). The source is placed at the location of the station NIL, and the depth surface shown is $z = 60$ km slice of the grid. The absolute maximum error does not exceed .35 seconds.

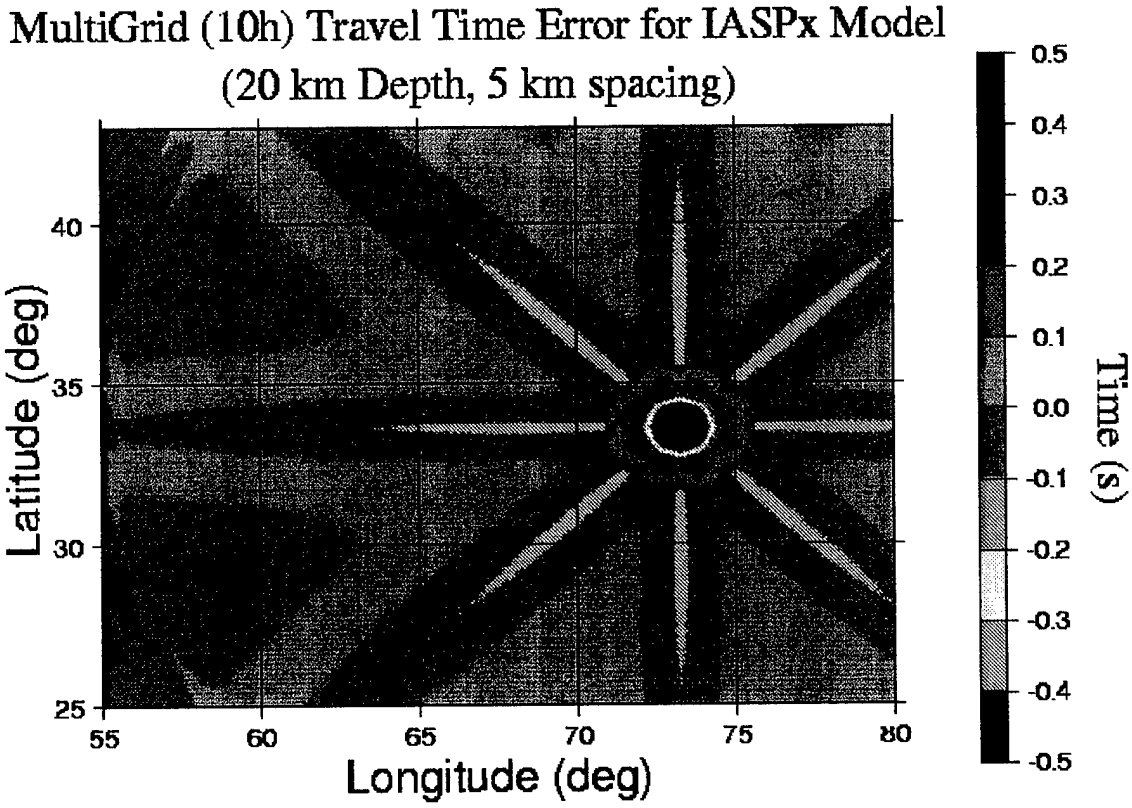

Figure 6: The travel time error between the P-L method and travel times from the IASP91 1-D velocity model. The source is placed at the location of the station NIL, and the depth surface shown is $z = 20$ km slice of the grid. Errors in the majority of the grid do not exceed .3 seconds; the larger errors near the station are due to the inexact times produced by our IASP91 analytic solution.

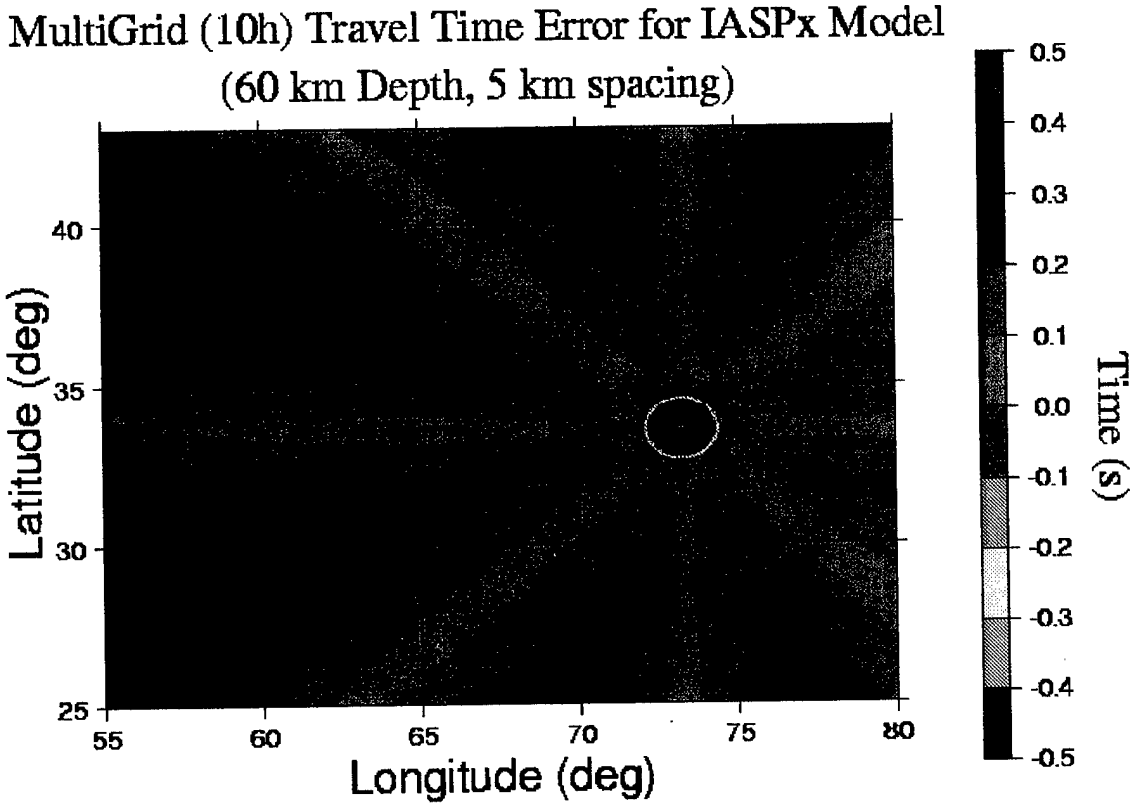

Figure 7: The travel time error between the P-L method and travel times from the IASP91 1-D velocity model. The source is placed at the location of the station NIL, and the depth surface shown is the $z = 60$ km slice of the grid. Errors in the majority of the grid do not exceed .4 seconds; the larger errors near the station are due to the inexact times produced by our IASP91 analytic solution.

The first arriving phase may be P_g (or some other purely crustal phase), P_n (head wave along the Moho discontinuity), or mantle P (i.e., rays turning or originating below the Moho), depending on the event location with respect to the station. By default, the P-L algorithm computes first-arrival travel times.

To compute a travel time table for P_g or P_n, whether or not it is first, we modify the velocity models input to the P-L in certain ways. To produce P_g travel times, we modify the velocity throughout the mantle to be very small, such that the first arrival to a surface station from any event in the crust will be P_g. (Strictly, it will be a crustal phase of some sort, which is our operational definition of P_g for the purposes of regional event location). The travel time grid produced in this way will have meaningless travel times at grid points (hypocenters) in the mantle. We edit the table to change these to minus 1.0 seconds, the signal to the grid-search location code that the travel time is undefined.

To compute P_n times, we modify the model differently. At each horizontal location (i.e., one column of the velocity model grid) the mantle velocity is made constant with depth and equal to the P_n velocity, i.e., model cells deeper in the mantle are given the same velocity as the shallowest mantle cell. Furthermore, the flattening transformation is not applied to the mantle cells, which would introduce a velocity gradient with depth. In this way, the first arriving phase from any event in the crust will be either P_g or P_n; rays will not turn in the mantle. The resulting travel time grids are then edited in two ways. First, points in the mantle are changed to -1.0. Second, if the travel time for a point in the crust is greater than or equal to the P_g time, that point is also assigned -1.0 seconds. This eliminates P_g times from the P_n table. It also eliminates P_n as a secondary arrival behind P_g, but this only occurs over a limited distance range from a station (between critical and cross-over distances) and, in any case, the ability to observe secondary P_n is difficult in practice.

After the complete set of phase travel time tables are calculated for the Pakistan regional model, three (P, P_g, P_n) per station, they are used in computing the objective function that is optimized by our grid-search location algorithm.

2.2 Task 2: Grid-Search Location Algorithm

The other key component of our location algorithm besides travel time computation is an inversion method to estimate the location of an event from observed arrival times. Our algorithm finds maximum likelihood estimates of the hypocenter, origin time, and data variance scale factor of the data errors. Under a fairly general probability model of the errors, maximizing the likelihood corresponds to minimizing the norm of arrival time residuals, i.e. a data "misfit" objective function.

The hypocentral parameters of a seismic event are a three-dimensional position vector $\mathbf{x}$ and an origin time t. Let $\mathbf{d} = (d_1, d_2 \ldots, d_n)$ be an n-dimensional vector of arrival time data from a seismic network picked from various seismic phases. The event location problem may

be expressed as

$$d_i = t + T_i(\mathbf{x}) + e_i, \quad i = 1, \ldots, n \tag{3}$$

where T_i is a travel time function (traveltime table) for the ith datum and e_i is an error with respect to this function. The index i counts over both stations and phase types (P_g, P_n, etc.), including only those combinations that have been actually observed (i.e., completeness of data coverage is not assumed).

A likelihood function is determined by the joint probability density function (p.d.f.) of the arrival time data, which in turn is determined by a probability model of the data errors. Our formulation assumes that the errors are statistically independent and, following Billings *et al.* (1994), that each is distributed with a "generalized Gaussian" p.d.f. For simplicity we consider here only the Gaussian case. Further, following earlier formulations of the event location problem (e.g. Jordan and Sverdrup, 1981), we assume that the error variances, σ_i^2, are known in a relative sense and write

$$\sigma_i = \sigma \nu_i \tag{4}$$

where the ν_i are given but the universal scale parameter, σ, is unknown. Under these assumptions, the likelihood function is given by

$$L(\mathbf{x}, t, \sigma; \mathbf{d}) = \frac{1}{(2\pi)^{n/2} \sigma^n \prod_{i=1}^n \nu_i} \exp\left\{-\frac{1}{2\sigma^2} \Psi(\mathbf{x}, t; \mathbf{d})\right\} \tag{5}$$

where Ψ is a 'data misfit' function:

$$\Psi(\mathbf{x}, t; \mathbf{d}) = \sum_{i=1}^{n} \left(d_i - t - T_i(\mathbf{x})\right)^2 / (\nu_i)^2. \tag{6}$$

The maximum likelihood estimates of the unknown parameters are the values that maximize L. We denote these estimates as $\mathbf{x}^{\text{ml}}$, t^{ml}, and σ^{ml}. The maximization may be subjected to prior constraints on the parameters. In our current implementation, we assume hard bounds on focal depth (z) and the scale variance:

$$0 \leq z \leq z^{\max}$$
$$\sigma^{\min} \leq \sigma \leq \sigma^{\max}.$$

We place no restrictions on latitude, longitude, or origin time.

Our grid search algorithm obtains the maximum likelihood estimates of the hypocentral parameters ($\mathbf{x}^{\text{ml}}$ and t^{ml}) and the p.d.f. scale parameter (σ^{ml}), as defined above. The algorithm computes a "reduced" likelihood function, $\tilde{L}$, at each point of a 3-D grid of hypocenters. This function is defined as

$$\tilde{L}(\mathbf{x}; \mathbf{d}) = \max_{t,\sigma} L(\mathbf{x}, t, \sigma; \mathbf{d}). \tag{7}$$

With $\mathbf{x}$ fixed, maximizing L with respect to origin time t corresponds to *minimizing* Ψ with respect to t, which is achieved by setting t to a weighted sum of the arrival residuals, $d_i - T_i(\mathbf{x})$. The maximizing σ is a weighted r.m.s. residual.

Following previous workers (e.g. Dreger *et al.*, 1998), we construct the search grid of hypocenters as a set of sub-grids of increasing fineness. In our algorithm, each grid is in a cylindrical coordinate system, i.e. sampled in distance and azimuth from some point and in depth. The azimuth sampling varies with distance to approximately equalize radial and angular sampling in kilometers. The first 6 grids used span approximately 6000 km in epicentral distance and are distributed to cover the entire globe (with some overlap) and focal depths from 0 to 750 km. The best hypocenter (largest value of $\widetilde{L}$) from these six grids is taken as the center a finer cylindrical grid of smaller aperture. After searching this finer grid, the algorithm generates a yet smaller, finer grid centered on the best hypocenter found thus far, and so on. The final maximum likelihood hypocenter, $\mathbf{x}^{\mathrm{ml}}$, is taken as the hypocenter achieving the largest reduced likelihood amongst all the points of all the grids searched. In the examples shown below, we used eight grid refinements in the recursive search, with grid spacing starting at 100 km, laterally and in depth, and shrinking to 0.1 km spacing for the final and densest grid. Since the examples were run with the regional Pakistan model, the global grids were bypassed: the largest grid was 3000 km in radius, extended well beyond the border of our model.

Our grid-search algorithm was initially written to accommodate only a spherically symmetric earth model. In this case, the travel time function, $T_i(\mathbf{x})$, is obtained by interpolating a 2-D travel time table, which samples travel time on a grid of epicentral distances and focal depths. We typically use the IASP91 tables for this purpose. For a 3-D earth model, $T_i(\mathbf{x})$ is evaluated by interpolating a 3-D travel time table, i.e. traveltime sampled on a 3-D grid. We extended our grid-search algorithm to use 3-D tables with the following features:

- Since the 3-D tables are computed on a Cartesian grid, with depth stretched via the flattening transformation, we applied the following steps before interpolating the travel time for a given event. First, the grid depths stored with the 3-D table were "unflattened" into true depths. Second, the relative location between a station and an event, in terms of spherical distance and azimuth, is converted to an approximate relative location in Cartesian coordinates. This relative location is then used to locate the event within the P-L grid for each station and phase.

- Given the event location in Cartesian coordinates, travel time is determined by trilinear interpolation between eight nodes. If any of the nodes has a travel time of -1.0, the travel time is treated as undefined, e.g. P_g for an event in the mantle.

- The travel time tables are quite large. For example, one P wave table for the Pakistan model even when resampled laterally at 20 km and truncated to 200 km in depth (as described below), contains about 500,000 numbers. Therefore, our algorithm is written

Table 1: Stations Used for Synthetic Data Tests

Name	*Latitude*	*Longitude*	*Description*
NDI	28.6833	77.2167	New Delhi (Delhi)
QUE	30.1883	66.9500	Quetta
DRP	31.7440	70.2028	Drazinda
SARP	31.9215	72.6718	Sargodha
SBDP	32.2997	70.8072	Shaikh Budin
THW	32.7943	71.7427	Thammewali
NIL	33.6500	73.2517	Nilore
CHCP	33.6583	73.2638	Chirah Chowk
CEP	33.8235	71.9090	Cherat
MAIO	36.3000	59.4945	Mashhad
ASH	37.9500	58.3500	Ashgabat (Ashkhabad)
KAT	39.2000	56.2667	Gyzylarbat (Kizyl-Arvat)
KSH	39.5167	75.9731	Kashi (Kashgar)
FRU	42.8333	74.6167	Bishkek (Frunze)

to store only a portion of a table at a time in a series of cache memory arrays. The appropriate table file is revisited when a new portion of a table is needed, overwriting the oldest cache array.

2.3 Task 3: Application to Synthetic Data

We applied our grid-search location algorithm to various hypothetical events in our Pakistan model region. The objective of these numerical experiments was mainly to test that the extension of our location algorithm to 3-D travel time tables was correct. The examples also serve to demonstrate the need for calibrated 3-D travel time information in areas of complex crustal structure and the location biases that are induced when global travel time tables are used in such areas.

For each hypothetical event, noise-contaminated synthetic arrival times were generated at 14 stations in the model region (see Table 1), and then the location algorithm was applied to these data to estimate the "true" location. The synthetic data were calculated from the 3-D travel time tables generated by running the P-L algorithm on our 3-D Pakistan model. Each synthetic arrival time was the sum of the model-based travel time, as interpolated from the appropriate 3-D table, an assumed origin time, and a zero-mean pseudo-random number to simulate a "picking error."

The 3-D travel time tables for this purpose were generated with a single-grid version of

Table 2: Location Errors for Crustal Events

True location			*No. of*	*Epicenter error (km)*		*Depth error (km)*	
lat.	*lon.*	*depth*	*data*	*2-D*	*3-D*	*2-D*	*3-D*
30	60	15	16	74.0	2.6	-15.0	2.9
30	65	15	19	97.6	6.9	-15.0	6.3
30	70	15	21	24.9	2.0	-10.2	0.2
30	75	15	22	17.7	1.3	-15.0	-1.0
35	60	15	16	13.1	2.9	-15.0	-2.4
35	65	15	24	10.7	1.9	-15.0	0.1
35	70	15	22	25.5	2.2	-15.0	2.4
35	75	15	21	21.9	1.1	-15.0	0.2
40	60	15	16	13.7	1.8	-15.0	-0.9
40	65	15	17	18.6	3.7	-15.0	0.1
40	70	15	20	27.1	1.6	-15.0	0.9
40	75	15	18	28.6	4.9	-15.0	8.3

P-L using a grid spacing of 5 km. Two tables for each station were generated: P_g and first arrival P. In the raytracing, the grids extended to a depth of 410 km and 80 km for P and P_g, respectively. The 3-D tables output by P-L were resampled and truncated in depth before using them in the grid-search algorithm. They were resampled with a horizontal spacing of 20 km laterally; the depth spacing of 5 km was retained. The P tables were truncated to a maximum depth of 200 km. The 80 km depth maximum for the P_g tables was retained. By truncating the P tables to 200 km, we eliminate event focal depths for which the raypath to one or more stations might dive below the 410 limit used in the raytracing.

The synthetic data set for a given event comprised P and P_g times at a subset of the 14 stations in Table 1. The subset was determined by some rules stating when a phase is observed as a function of source-receiver distance (Δ) and event depth. For crustal events, we arbitrarily assumed that P was observed for $\Delta \geq 2.5$ degrees, and P_g was observed when $\Delta \leq 7.5$ degrees. For mantle events, P_g is never observed and P is observed at all distances. The noise standard deviation was set to 0.5 sec for P and 0.25 sec for P_g.

While the synthetic data were generated with 3-D travel time tables, we performed the location of each event two ways: using the same 3-D tables, and using the 2-D IASP91 tables. Table 2 summarizes the event mislocations resulting each way for events at a depth of 15 km. Twelve such events were assumed, on a 5 by 5 degree grid over the model region. The leftmost columns of the table gives the "true" hypocenter of each event. The number of data used in the location of the event is next, followed by the location errors. The columns labeled "2-D" are the errors when IASP91 tables are used in the grid search, and those labeled "3-D"

Table 3: R.M.S. Residuals for Crustal Events

True Location			*No. of*	*RMS Resid. (s)*	
lat.	*lon.*	*depth*	*Data*	*2-D*	*3-D*
30	60	15	16	1.091	0.299
30	65	15	19	2.476	0.235
30	70	15	21	1.712	0.256
30	75	15	22	1.480	0.286
35	60	15	16	2.055	0.261
35	65	15	24	2.343	0.271
35	70	15	22	1.463	0.235
35	75	15	21	2.377	0.243
40	60	15	16	2.007	0.291
40	65	15	17	2.561	0.255
40	70	15	20	2.202	0.274
40	75	15	18	4.491	0.251

are when the 3-D Pakistan tables are used. We see immediately that the location errors are much smaller when the correct 3-D tables are used. The horizontal mislocation errors are then very small, the largest being about 6.9 km and most less than 3 km. The errors in focal depth are also generally small, the largest being 8.3 km and many less than one km. Since the correct tables were used in this case, the mislocations are due only to the noise, i.e. picking errors, in the cdata. Given the size of the picking errors and the large number of data at local and regional distances, it is expected that the picking errors do not induce large event mislocations, which is what we see. However, turning now to the columns headed "2-D", we see that using IASP91 tables in the grid-search *does* induce large errors, despite the generally good coverage. Our Pakistan model differs from the IASP91 model by up to several seconds in travel time, which we see induces large epicentral errors varying from 10 to 100 km amomg the events. Many of the errors well exceed the desired 18 km for CTBT monitoring. The errors in focal depth resulting from using IASP91 tables are uniformly negative, with all but one located at the top of the search grid, i.e. surface focus.

Another comparison of the 2-D and 3-D locations is given in Table 3. This shows the r.m.s. arrival time residual resulting from each location run. When the correct 3-D tables are used, they vary between 0.2 and 0.3 sec, which is consistent with the assumed noise level. For the IASP91 locations, they are many times larger in every case, varying from 1 to over 4 seconds.

Tables 4 and 5 show analogous results for 12 hypothetical events at a focal depth of 100 km. Now each data set contains exactly one mantle P wave at each of the 14 stations. The

Table 4: Location Errors for Mantle Events

True location			*No. of*	*Epicenter error (km)*		*Depth error (km)*	
lat.	*lon.*	*depth*	*data*	*2-D*	*3-D*	*2-D*	*3-D*
30	60	100	14	18.4	4.3	7.1	-5.3
30	65	100	14	13.9	2.9	17.0	2.5
30	70	100	14	11.3	1.9	23.6	-5.7
30	75	100	14	14.8	1.9	19.4	-8.7
35	60	100	14	28.7	2.7	0.0	-1.5
35	65	100	14	21.3	0.7	-10.2	-22.6
35	70	100	14	9.9	3.2	4.6	-2.4
35	75	100	14	8.1	3.0	6.3	-3.8
40	60	100	14	12.6	4.0	-12.3	-0.9
40	65	100	14	23.0	2.8	0.0	-50.2
40	70	100	14	17.3	1.1	-49.5	-90.1
40	75	100	14	7.1	3.5	-100.0	9.9

use of 3-D tables in the location clearly yields smaller mislocations, but as dramatically as for shallow events. This particularly true for the depth mislocations, which for a few events are actually larger when the 3-D tables are used. We attribute this to the fact that focal is poorly constrained in any case for deep events below the network. As before, The r.m.s. residuals are consistently larger 2-D tables are used, but not by as large a factor.

3.0 CONCLUSIONS

Our focus during Phase I of this research project was to demonstrate the capabilities of a powerful seismic event location method which uses 3-D velocity models and body wave arrival times to estimate hypocenters. Experts in seismic monitoring have stated that the development of methods to improve hypocenter estimation for the regional seismic monitoring problem is a research priority of great importance (National Research Council Committee on Seismology report, 1997). Our research directly contributes to that effort through the development of a sophisticated technique to produce improved event locations from regional travel times and 3-D velocity models. The Phase I effort has produced a prototype algorithm for locating regional events with 3-D velocity models. This type of location method is not currently the norm at US monitoring agencies. The method incorporates sophisticated, grid-based ray tracing techniques and search algorithms to estimate event hypocenters. We have made significant progress on several technical objectives: 1) Improvement in the accuracy of the 3-D, Podvin-Lecomte grid-based travel time code and adaptation to the regional

Table 5: R.M.S. Residuals for Mantle Events

True Location			*No. of*	*RMS Resid. (s)*	
lat.	*lon.*	*depth*	*Data*	*2-D*	*3-D*
30	60	100	14	1.090	0.285
30	65	100	14	0.782	0.314
30	70	100	14	0.720	0.305
30	75	100	14	0.776	0.299
35	60	100	14	1.197	0.316
35	65	100	14	0.954	0.275
35	70	100	14	0.655	0.270
35	75	100	14	0.681	0.266
40	60	100	14	1.688	0.321
40	65	100	14	1.124	0.272
40	70	100	14	0.747	0.319
40	75	100	14	0.654	0.265

monitoring problem; 2) Adaptation of the maximum likelihood grid-based location method to the 3-D regional location problem; 3) Incorporation of secondary phases in hypocenter estimates; 4) Application to a set of synthetic events from a region of US monitoring concern to demonstrate the feasibility and potential of the method. There are still significant improvements and obstacles to be addressed before the technique can be used in an operational setting, and we will address these in our forthcoming Phase II proposal. However, we believe that the technique has significant potential to be useful in both monitoring seismology and passive underground facility characterization.

References

Billings, S.D., M.S. Sambridge and B.L.N. Kennett, 1994, Errors in hypocenter location: picking, model and magnitude dependence, *Bull. Seism. Soc. Am., 84*, 1978–1990.

Dreger, D., R. Uhrhammer, M. Pasyanos, J. Franck and V. Romanowicz, 1998, Regional and far-regional earthquake locations and source parameters using sparse broadband networks: a test on the Ridgecrest sequence, *Bull. Seism. Soc. Am., 88*, 1353–1362.

Group of Scientific Experts (GSE) Conference Room Paper 243 (1995), on-line paper detailing all aspects of the GSETT-3 test and current IDC operations, found at www.pidc.org.

Jordan, T. H. and K. A. Sverdrup (1981). Teleseismic location techniques and their application to earthquake clusters in the south-central Pacific, *Bull. Seism. Soc. Am., 71*, 1105–1130.

Lomax, A., P. Volant, C. Berge, and J. Virieux (1998), Probabilistic, grid-search earthquake location in three-dimensional media: Application to the Durance Network in the South of France, Shalheveth Freier 1st Intl. Workshop on Advanced Methods in Seismic Analysis, January, 1998, Dead Sea, Israel.

Moser, T.J. (1991), Shortest path calculation of seismic rays, *Geophysics*, 56, pp. 59-67.

Moser, T.J., T. Van Eck, and G. Nolet (1992), Hypocenter determ ination in strongly heterogeneous earth models uing the shortest path method, *J. Geophys. Res.*, 97, pp. 6563-6572.

Podvin, P. and I. Lecomte (1991), Finite difference computation of travel times in very contrasted velocity models: a massively parallel approach and its associated tools, *Geophys. J. Int.*, 105, pp. 271-284.

Research Required to Support Comprehensive Test Ban Treaty Monitoring (1997), Report from the National Research Council, National Academy Press, ISBN 0-309-05826-0.

Vidale, J. (1988), Finite difference calculations of travel times *Bull. Seismol. Soc. Amer.*, 78, pp. 521-526.

Wittlinger, G., G. Herquel, and T. Nakache (1993), Earthquake location in strongly heterogeneous media, *Geophys. J. Int.*, 115, pp. 759-777.